



Boosting the photoluminescence of 2D organic–inorganic perovskite films by mixing with polymers

Mostafa M. Abdelhamied^{1,2} · Yan Gao¹ · XiaoHong Li³ · Weiwei Liu¹

Received: 3 October 2021 / Accepted: 7 December 2021 / Published online: 22 December 2021
© The Author(s), under exclusive licence to Springer-Verlag GmbH, DE part of Springer Nature 2021

Abstract

Herein, Poly(4-Vinylpyridine) (PVP) and Poly(ethylene oxide) (PEO) mixed (PEA)₂PbI₄ films are fabricated by spin-coating method. The optical and SEM images exhibit improved morphology with more uniform and homogeneous surfaces after mixing PVP and PEO polymers, which increases with the concentrations of the polymers. XRD and FTIR measurements show that the crystal structure and functional group of the (PEA)₂PbI₄ film don't change after introducing the polymer. The optical bandgap of the polymer-mixed (PEA)₂PbI₄ films gradually increased with increasing the concentrations of PVP and PEO polymers. Moreover, the two-photon-pumped photoluminescence (TPL) has been boosted by 3.5 and 3.8 folds by mixing with 25% PVP and 25% PEO, respectively. Time-resolved PL measurements indicate that the PL lifetimes of the polymer-mixed (PEA)₂PbI₄ films have been increased, proving that the increased TPL emission is due to the improved crystalline quality and decreased trap states. This work provides an effective strategy to improve the crystalline quality and photoemission of the 2D perovskite films, which shows great promise for manufacturing high-performance optoelectronic devices based on 2D perovskites.

Keywords 2D Perovskites · Polymer · Photoluminescence boosting · Optoelectronic devices

1 Introduction

Recently, 3D hybrid organic–inorganic perovskites (HOIPs) have presented a great outlook for application in light-emitting devices, photodetectors, and solar cells [1–5]. However, the instability of 3D perovskites in an ambient environment still hinders the practical applications [6, 7]. Instead, 2D HOIPs are derived from 3D HOIPs to solve this issue due to their outstanding humidity resistance [8]. 2D HOIPs possess

a general chemical formula (RNH₃)₂(CH₃NH₃)_{n-1}M_nX_{3n+1}, where R is a long-chain organic group, M represents a metal cation, X indicates a halide anion, and n refers to the number of octahedrons layers among the organic spacers [9–11]. The shrinking of 3D HOIPs to 2D fetches individual properties, such as stronger quantum confinement, a greater tenability, and a higher exciton binding energy owing to the multiple-quantum-well structure [12–15]. Accordingly, 2D HOIPs have opened new avenues for optoelectronic applications [16–19].

Although 2D perovskite has several excellent advantages, these materials still suffer from severe trap states [20, 21]. This issue remains a challenge for obtaining high-performance optoelectronic devices based on 2D perovskites. Accordingly, a lot of works have been suggested for enhancing photoemission by improving the surface morphology and crystalline grains. For example, Song et al. [22] improved the surface morphology of 2D perovskite using UV-light illumination during growth, which helps decrease trap-assisted recombination and improves the PL emission. Yang et al. used small-molecule trioctylphosphine oxide for coating the surface of quasi-2D perovskite film, reducing the non-radiative recombination and increasing the green

✉ Mostafa M. Abdelhamied
m_elbana52@yahoo.com

✉ Weiwei Liu
lwhust@hust.edu.cn

¹ Wuhan National Laboratory for Optoelectronics and School of Physics, Huazhong University of Science and Technology, Wuhan 430074, China

² Radiation Physics Department, National Center for Radiation Research and Technology (NCRRT), Egyptian Atomic Energy Authority (EAEA), Cairo, Arab Republic of Egypt

³ Hubei Key Laboratory of Optical Information and Pattern Recognition, Wuhan Institute of Technology, Wuhan 430205, China

emission [23]. Besides, polymer's addition is also effective for improving the stability and photoemission of the perovskites. As the polymer can tune the surface morphology and grain size, reducing the trap state and enhancing the radiative recombination [24, 25]. Chang et al. improved the PCE by 25% after adding 1, wt.% of PEG into perovskite, improving the surface morphology and controlling in size and gathering of crystals [26]. Further, Yavari et al. displayed that inserting a fluffy interlayer of PVP polymer among the perovskite and the hole transport layer (HTL) decreased the non-radiative recombination, increasing the photoemission [27]. Despite polymer mixing was widely studied in 3D perovskites, the effect of polymer mixing on optical properties of 2D HOIPs still needs further investigation.

In this work, we propose to boost the photoluminescence of 2D HOIP films by mixing them with polymers. We fabricate Poly(4-Vinylpyridine) (PVP) and Poly(ethylene oxide) (PEO) mixed $(\text{PEA})_2\text{PbI}_4$ films by spin-coating method. The polymer-mixed $(\text{PEA})_2\text{PbI}_4$ films exhibit more uniform and homogeneous surfaces compared with the pristine films, indicating an improved morphology by polymer mixture. We investigate the two-photon-pumped photoluminescence (TPL) of the fabricated $(\text{PEA})_2\text{PbI}_4$ films, which can be attributed to the exciton recombination. Moreover, we observe an enhancement of the (TPL) polymer-mixed $(\text{PEA})_2\text{PbI}_4$ films, by 3.5 and 3.8 folds, respectively, with 25% PVP and 25% PEO. The time-resolved PL measurement indicates that the PL lifetime of the polymer-mixed $(\text{PEA})_2\text{PbI}_4$ films has been increased, indicating that the increased TPL emission is due to the improved crystalline quality and decreased trap states.

2 Experimental part

2.1 Materials

All powders and solvents are applied as received without further refinement. Phenylethylamine iodide (PEAI, MW 249) was purchased from Dyesol and Lead iodide (PbI_2 , MW 461) from Alfa Aesar. Poly(4-Vinylpyridine) (PVP, MW 58 000), Polyethylene Oxide (PEO, MW 100 000), N, N-dimethylformamide (DMF) (anhydrous, 99.8%) were obtained from Sigma-Aldrich. Toluene (99.8%) was bought from Sigma-Aldrich.

2.2 Preparation of $(\text{PEA})_2\text{PbI}_4$ films

The 2D $(\text{PEA})_2\text{PbI}_4$ films were synthesized by spin-coating method, as illustrated in Fig. 1a [28]. Firstly, the glass substrates were cleaned by consecutive ultrasonic, thereby in detergent, acetone, deionized water, and ethanol. After that, the substrates were dried at 60 °C for 10 min. And then,

the powders of PbI_2 (461 mg, 1 mol) and PEAi (498.4 mg, 2 mol) were mingled and resolved in 1.0 mL of DMF at 80 °C via a magnetic stirrer for one hour; 25 μL of the solution was dropped onto the clear substrate for two-step spin coating (1000 rpm, 10 s in the first step, and 3000 rpm, 30 s in the second step). The second step was used to spread the perovskite solution over all the substrate and make the film more homogeneous. In addition, 15 μL of toluene was dropped during the second spinning agenda onto the substrate after 10 s from the onset of the spinning process to make the film more homogeneity. Lastly, the films were annealed at 80 °C for 10 min on a hotplate. To prepare the $(\text{PEA})_2\text{PbI}_4$ films mixed with polymers, Poly(4-Vinylpyridine) (PVP) and Poly(ethylene oxide) (PEO) powders were, respectively, dissolved in DMF to form the polymer solutions (18 mg/mL). Subsequently, PVP and PEO solutions with different concentrations (5%, 15%, and 25%) were, respectively, added to the $(\text{PEA})_2\text{PbI}_4$ solution and then mixed via magnetic stirrer for one hour. The $(\text{PEA})_2\text{PbI}_4$ films mixed with polymers were also prepared by the same spin-coating procedures.

2.3 Physical characterization

The surface morphology of the pristine and the mixed $(\text{PEA})_2\text{PbI}_4$ films was studied using scanning electron microscopy SEM (SEM, Nova NanoSEM 450) with an optical microscope (IX73, Olympus). The structural properties of the films were demonstrated by using XRD (XRD, Empyrean). UV–Vis spectrometer has been carried out in the range from 400 to 800 nm to determine the absorption spectra of the samples. Steady-state two-photon absorption induced photoluminescence (TPL) measurements were performed through utilizing a Ti: sapphire oscillator (Vitara, Coherent, 800 nm, ~ 30 fs, 80 MHz) for excitation. The TPL signal was directed to a spectrometer (Andor 193i) for spectral measurement or a TCSPC system (PicoHarp 300, PicoQuant) for lifetime measurement.

3 Results and discussion

Figure 1b and c show the optical microscope images of the as-prepared and polymer-mixed $(\text{PEA})_2\text{PbI}_4$ films. It can be observed that the $(\text{PEA})_2\text{PbI}_4$ films have been formed with great grain sizes and inhomogeneous surfaces. In contrast, the films become with a regular form and uniform surfaces after incorporating PVP and PEO polymers inside the 2D perovskite films. Figure 2a and b show the SEM image of the pristine and polymer-mixed $(\text{PEA})_2\text{PbI}_4$ films with different concentrations of PVP and PEO, respectively. It is observed that the pristine $(\text{PEA})_2\text{PbI}_4$ film manifests large grains with average sizes between 4 and 12 μm , where some

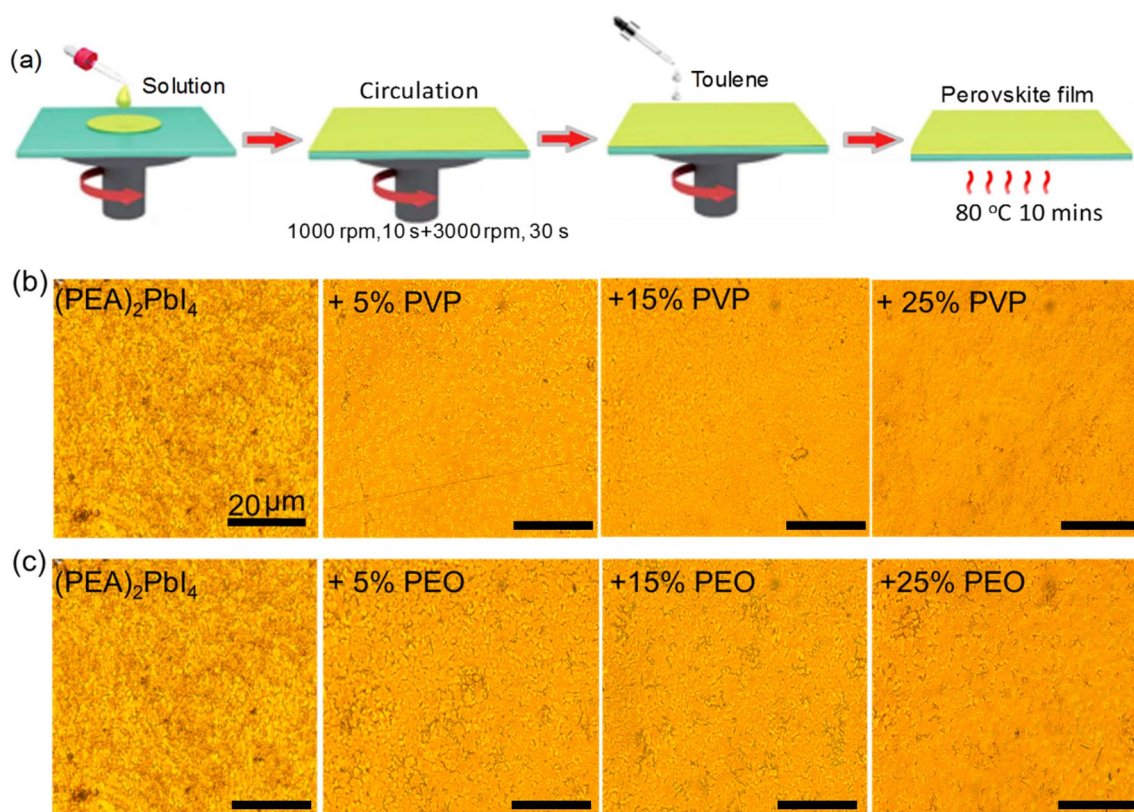


Fig. 1 **a** Schematic diagram for the spin coating of $(\text{PEA})_2\text{PbI}_4$ films. **b** Optical microscope images of the pristine $(\text{PEA})_2\text{PbI}_4$ film and the 5%-, 15%-, 25%-PVP mixed $(\text{PEA})_2\text{PbI}_4$ films. **c** Optical microscope

images of the pristine $(\text{PEA})_2\text{PbI}_4$ film and the 5%-, 15%-, 25%- PEO mixed $(\text{PEA})_2\text{PbI}_4$ films

grains are linked with their neighbors to form larger-sized islands. Moreover, the surface of the pristine film is inhomogeneous and contains several bores and cracks. However, the morphology of the mixed films with different concentrations of PVP and PEO appears more uniform, without pinholes and cracks. Obviously, the amount of grain boundary is decreased after adding PVP and PEO polymer, which is a benefit for reducing the defect density and improving the surface morphology [29, 30]. This effect agrees well with many previously reported studies to find better quality perovskite films, which facilitates the improvement of optoelectronic performance [30, 31]. Additionally, one can observe that increasing the concentrations of PVP and PEO polymers leads to a great improvement in the surface morphology of the perovskite film.

Figure 2c and d display the XRD pattern of the pristine and polymer-mixed $(\text{PEA})_2\text{PbI}_4$ films, respectively. The pristine $(\text{PEA})_2\text{PbI}_4$ film show strong peaks located at $2\theta = 10.67^\circ$, 16.11° , 21.6° , 26.6° , 32.7° , and 38.4° respectively, which correspond to the $(00l)$ of the 2D layered structure, which agrees well with the reported results [32–34]. In particular, the XRD patterns of the $(\text{PEA})_2\text{PbI}_4$

films remain unvaried after mixing with different concentrations of PVP and PEO, which indicate that mixing of polymer does not change the crystal structures of the 2D perovskites. In addition, the stronger and sharper peaks of the XRD patterns for the polymer-mixed $(\text{PEA})_2\text{PbI}_4$ films imply an improvement of the crystalline and molecular ordering of the intermediate phase induced by the long-chain polymer. For further confirmation, the average crystallite size (D) is calculated of the pristine and mixed $(\text{PEA})_2\text{PbI}_4$ films for the main peak (0010) using the following relation (listed in Table 1) [35]:

$$D = \frac{0.9\lambda}{\beta \cos\theta}$$

It is found that the crystal size of the pristine film was increased after introducing PVP and PEO polymers. The increase in crystal size is able to form a regular film with lower grain boundaries and pinholes on the surface and leads to high optoelectronic performance. Additionally, the dislocation density (δ) is also an important parameter to reveal the degree of crystallinity, which is deduced from the following relation [36]:

Fig. 2 **a** SEM images of the pristine $(\text{PEA})_2\text{PbI}_4$ film and the 5%-, 15%-, 25%-PVP mixed $(\text{PEA})_2\text{PbI}_4$ films. **b** SEM images of the pristine $(\text{PEA})_2\text{PbI}_4$ film and the 5%-, 15%-, 25%-PEO mixed $(\text{PEA})_2\text{PbI}_4$ films. **c** XRD patterns of the pristine $(\text{PEA})_2\text{PbI}_4$ film and the 5%-, 15%-, 25%-PVP mixed $(\text{PEA})_2\text{PbI}_4$ films. **d** XRD patterns of the pristine $(\text{PEA})_2\text{PbI}_4$ film and the 5%-, 15%-, 25%-PEO mixed $(\text{PEA})_2\text{PbI}_4$ films

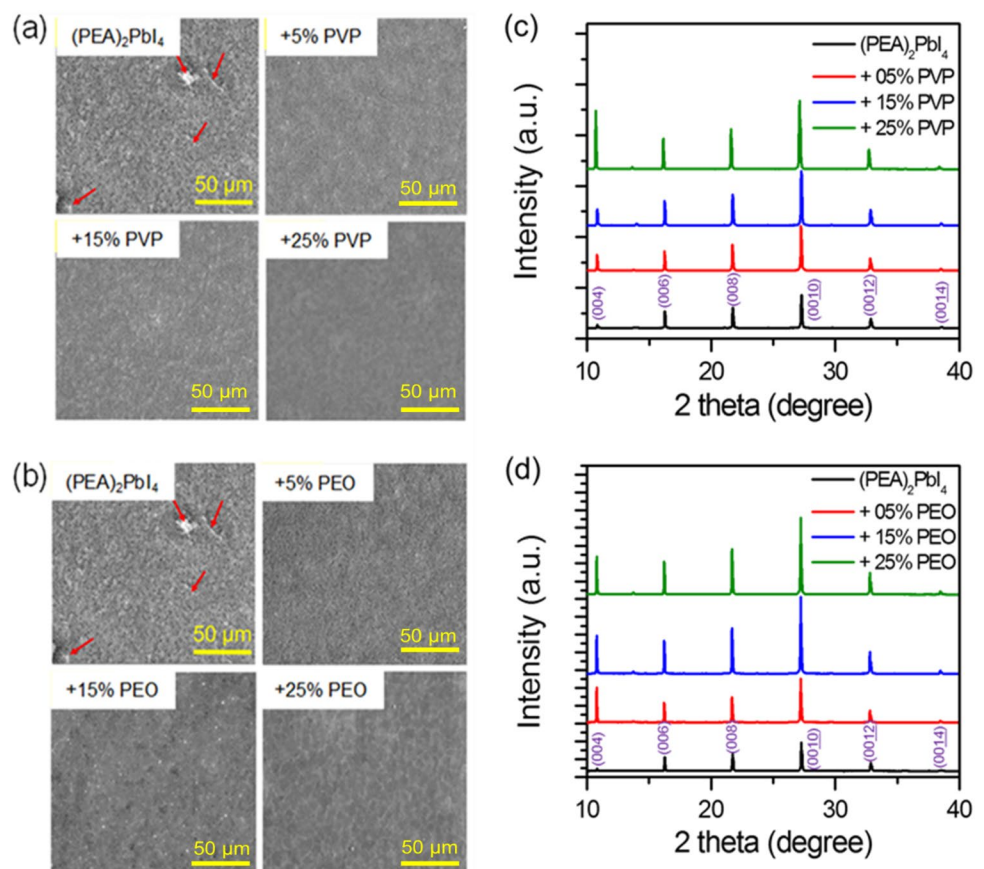


Table 1 The quantitative induced changes in the microstructural parameters of the $(\text{PEA})_2\text{PbI}_4$ films after introducing different concentrations of PVP and PEO polymers

	$(\text{PEA})_2\text{PbI}_4$	+5% PVP	+15% PVP	+25% PVP	+5% PEO	+15% PEO	+25% PEO
Crystal size [nm]	64.53	68.03	69.29	70.31	68.42	69.47	70.49
dislocation density [10^{-4} lines/ m^2]	2.41	2.16	2.08	2.02	2.14	2.07	2.01

$$\delta = \frac{1}{D^2}$$

We found that the average dislocation density of the pristine film was 1.44×10^{-5} , and, respectively, decreased to 1.154×10^{-5} and 1.164×10^{-5} lines/ m^2 of the $(\text{PEA})_2\text{PbI}_4/25\%\text{PVP}$ and $(\text{PEA})_2\text{PbI}_4/25\%\text{PEO}$ (listed in Table 1). These results confirm enhancing the crystallinity after introducing PVP and PEO polymers, which decreases the defect state and hence the trap states. And this is an important aspect of photoluminescence improvement.

FTIR analysis was performed to describe the chemical interactions between the $(\text{PEA})_2\text{PbI}_4$ and polymers. Figure 3a and b show the FTIR of the non-mixed and mixed films with different concentrations of PVP and PEO, respectively. It is observed that the pristine film has absorption

peaks at ~ 2847.64 , 2912.68 , and 3018.34 cm^{-1} , corresponding to the stretching or bending vibrations of $-\text{CH}_3$ and $-\text{CH}_2$ [37]. Further, the absorption bands which are located at about 3061.59 and 3160 cm^{-1} are referred to as N–H stretching vibrations [38]. Additionally, the FTIR spectra of the mixed films with different concentrations of PVP and PEO polymers are well similar to the spectrum of the pristine perovskite film. Nevertheless, the peaks are shifted to a lower wavenumber, and the intensity is decreased after introducing both polymers to the original film. This could be attributed to the interaction between the polymers and the perovskite molecules.

Figure 4a shows the absorption spectra of the pristine and PVP-mixed $(\text{PEA})_2\text{PbI}_4$ films. All films manifest a narrow absorption peak at 518 nm, which agrees with the excitonic absorption of $(\text{PEA})_2\text{PbI}_4$ [39]. Further, the figure also

Fig. 3 **a** FTIR of the pristine (PEA)₂PbI₄ film and the 5%-, 15%-, 25%-PVP mixed (PEA)₂PbI₄ films. **b** FTIR of the pristine (PEA)₂PbI₄ film and the 5%-, 15%-, 25%-PEO mixed (PEA)₂PbI₄ films

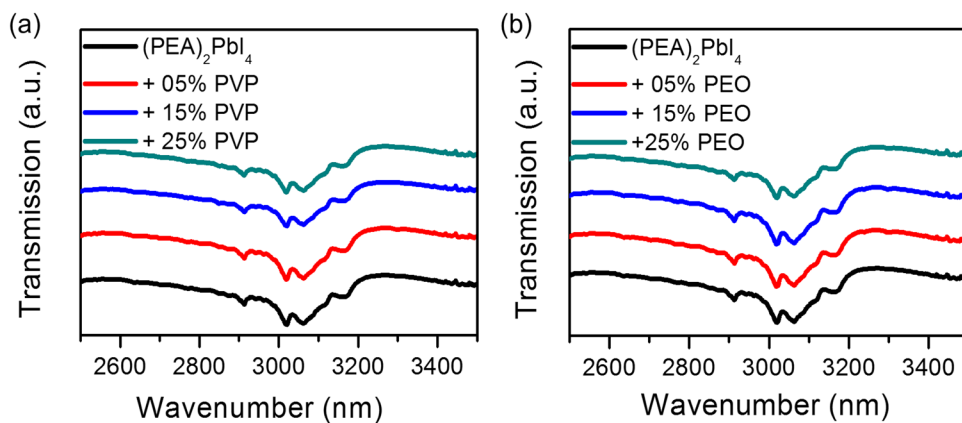
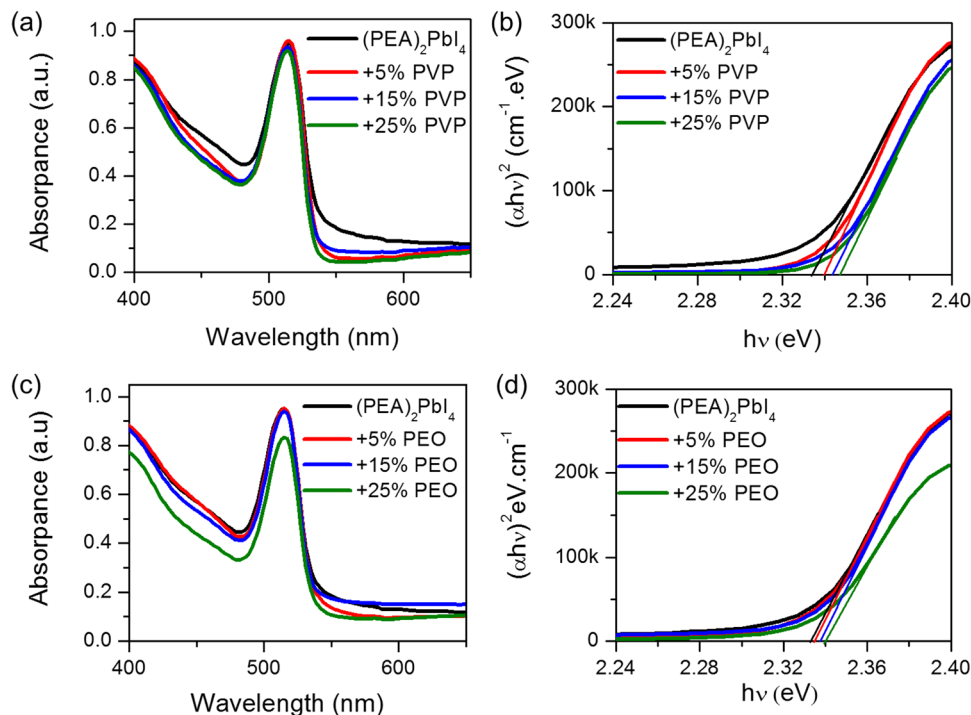


Fig. 4 **a** Absorption spectra, and **b** the corresponding Tauc plots of the pristine and PVP-mixed (PEA)₂PbI₄ films. **c** Absorption spectra, and **d** the corresponding Tauc plots of the pristine and PEO-mixed (PEA)₂PbI₄ films



shows that introduction of polymers into the perovskite layer leads to a slight decrease in the light absorption, which may be attributed to increasing the crystal size of the polymer-mixed films. In addition, the optical bandgap (E_g) of the pristine and polymer-mixed (PEA)₂PbI₄ film is extracted using Tauc’s equation [40, 41]:

$$\alpha h\nu = B(h\nu - E_g)^n$$

where α refers to the absorption coefficient, the factor n is 1/2 for a direct allowed transition, and B represents the absorption edge parameter. Figure 4b is utilized for determining the perovskite bandgap as a function of the PVP concentrations. It was found that the optical bandgap of the (PEA)₂PbI₄ film is 2.334 eV, which gradually increased with

increasing the concentrations of PVP polymers. Thus, the bandgap is enhanced to 2.348 of the (PEA)₂PbI₄/25% PVP. This change may be due to increasing the crystallinity and shifting of the Pb²⁺ 4f core-level peak, which dominates the bandgap [42]. Similar results were obtained for the PEO-mixed (PEA)₂PbI₄ films, as shown in Fig. 4c and d, in which the bandgap of the (PEA)₂PbI₄/25% PEO increased to 2.343 eV.

To investigate the photoemission properties, the PL images of the pristine and polymer-mixed (PEA)₂PbI₄ films are measured for comparison. Figure 5a and b show the PL images of the pristine and mixed (PEA)₂PbI₄ films with different concentrations of PVP and PEO, respectively. The figures manifest that (PEA)₂PbI₄ film holds strong fluorescence due to the high exciton binding energy, which leads to rapidly radiative recombination

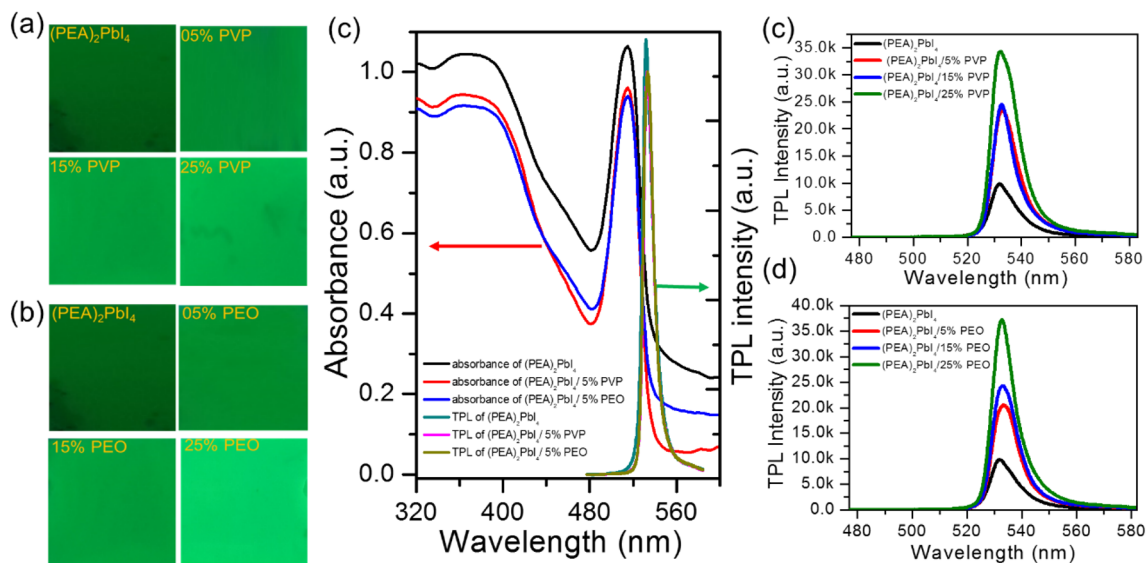


Fig. 5 **a** PL images, and **b** the TPL spectra of the pristine and PVP-mixed (PEA)₂PbI₄ films. **c** Linear absorption and TPL spectra of the (PEA)₂PbI₄, (PEA)₂PbI₄/5% PVP, and (PEA)₂PbI₄/5% PEO, films.

d PL images, and **e** the TPL spectra of the pristine and PEO-mixed (PEA)₂PbI₄ films

and enhanced PL [43]. Moreover, the green PL emission gradually increases with increasing the concentrations of PVP and PEO polymers. Figure 5c presents the normalized absorption and TPL spectra of the pristine (PEA)₂PbI₄, (PEA)₂PbI₄/5% PVP, (PEA)₂PbI₄/5% PEO, respectively. It is observed that these spectra are well overlapped, and the absorption onset is complemented by almost identical with PL spectra, which demonstrates that the E_g was maintained. For quantitative characterization, the TPL spectra of the pristine and mixed (PEA)₂PbI₄ films with different concentrations of PVP were measured, as shown in Fig. 5d. The TPL spectra display a homogenous PL peak located at ~ 535 nm, which is consistent with the reported results [44, 45]. More importantly, the photoemission intensity of the PVP-mixed (PEA)₂PbI₄ films increases gradually with the concentration of PVP, which has been increased by 3.5 folds after incorporating by 25%-concentration PVP. Figure 5e also shows that mixed with PEO is also beneficial for increasing the PL emission of the (PEA)₂PbI₄ films, and the TPL intensity of the (PEA)₂PbI₄ film has been increased by 3.8 folds. As analyzed above, the pyridine part (side chain) in PVP polymer can passivate lead ions which are caused by misalignment surface defects and can fill the iodine on the surface of the perovskite film vacancy trap. Therefore, it leads to reducing the trap state and enhancing the radiative recombination and PL [42, 46]. Besides, the PEO polymer chemically interacts with lead ions on the perovskite surface, which leads to passivating the undercoordinated defect states. As a result, the trap state is decreased, thus boosting the radiative recombination and PL emission [47].

We also measured the power-dependent TPL intensities for the (PEA)₂PbI₄ films to reveal the photoemission nature. Figure 6a–c show the power-dependent TPL spectra for the pristine, PVP-mixed, and PEO-mixed (PEA)₂PbI₄ films, respectively. Correspondingly, Fig. 6d–f show plots of the TPL intensity as a function of the excitation power. In the large-area (PEA)₂PbI₄ crystals, the surface traps will lead to a bimolecular recombination process, which results in a super-quadratic power dependence of the TPL on the excitation power [48, 49]. However, in this work, we can observe that for all the (PEA)₂PbI₄ films, the power-dependent TPL intensities are quadratic-dependent on the excitation power, which can well prove that the TPL emission is originated from the exciton recombination in the pristine and polymer-mixed (PEA)₂PbI₄ films [45, 48]. Therefore, we can conclude that the TPL enhancement in the polymer-mixed (PEA)₂PbI₄ films do not originate from the bimolecular recombination process but due to the improved crystalline quality and decreased traps.

In order to demonstrate the mechanism for the TPL enhancement, the PL lifetimes of the pristine and polymer-mixed (PEA)₂PbI₄ films were measured. Figure 7a and b display the time-resolved PL decay traces for the pristine, PVP-mixed, and PEO-mixed (PEA)₂PbI₄ films, respectively. As reported, the radiative recombination of 2D perovskites can be constructed from the intrinsic exciton recombination and the trap-states recombination [50]. A bi-exponential decay function is used to fit the PL decay curves [22].

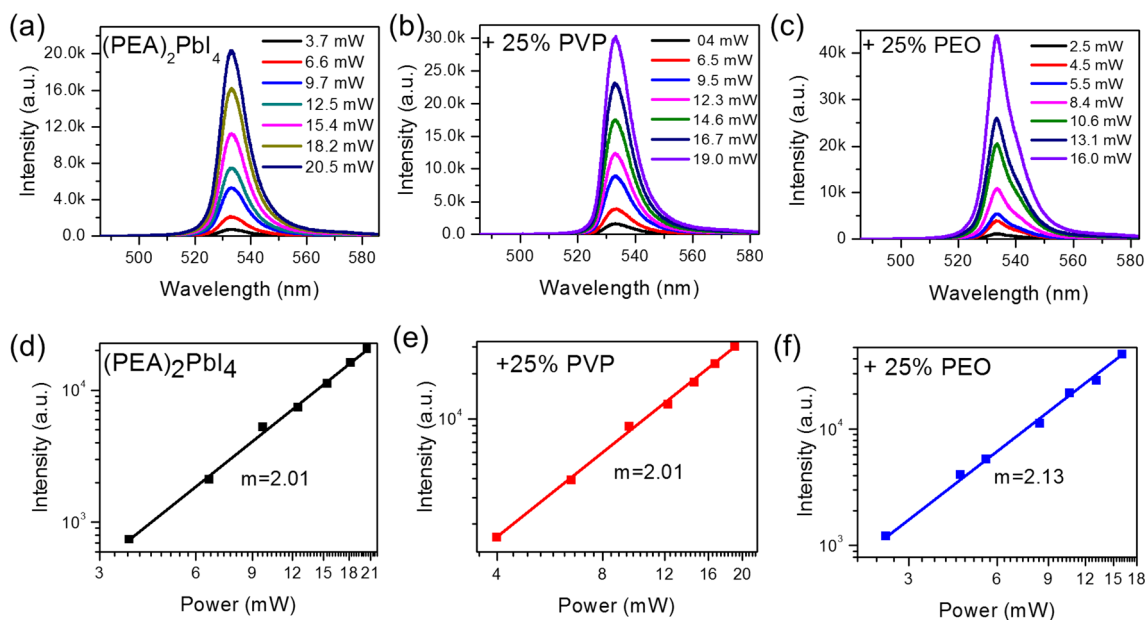
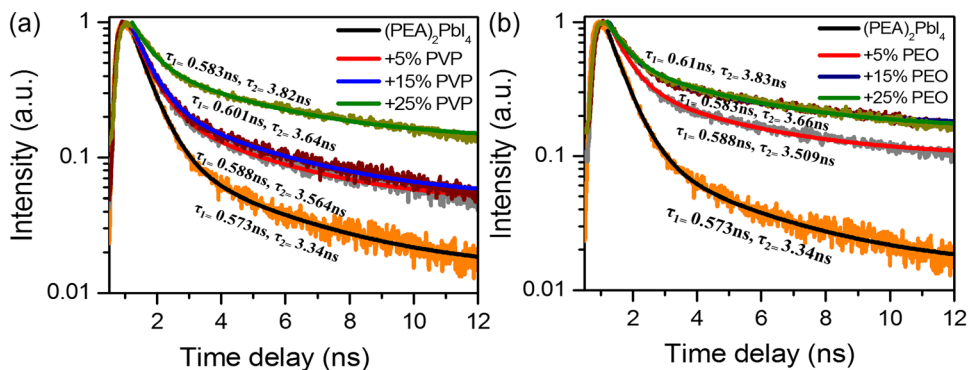


Fig. 6 Power-dependent TPL spectra for **(a)** pristine $(\text{PEA})_2\text{PbI}_4$ film, **b** 25%-PVP mixed $(\text{PEA})_2\text{PbI}_4$ films, and **(c)** 25%-PEO mixed $(\text{PEA})_2\text{PbI}_4$ films. Plots of the TPL intensity as a function of the excitation power for **(d)** pristine $(\text{PEA})_2\text{PbI}_4$ film, **e** 25%-PVP mixed $(\text{PEA})_2\text{PbI}_4$ films, and **f** 25%-PEO mixed $(\text{PEA})_2\text{PbI}_4$ films

Fig. 7 a Time-resolved PL decay traces for pristine $(\text{PEA})_2\text{PbI}_4$ film and the 5%-, 15%-, 25%-PVP mixed $(\text{PEA})_2\text{PbI}_4$ films. **b** Time-resolved PL decay traces for pristine $(\text{PEA})_2\text{PbI}_4$ film and the 5%-, 15%-, 25%-PEO mixed $(\text{PEA})_2\text{PbI}_4$ films



$$I(t) = A_1 \exp\left(\frac{-t}{\tau_1}\right) + A_2 \exp\left(\frac{-t}{\tau_2}\right)$$

where A_1 and A_2 represent the decay amplitude, the fast part τ_1 refers to the surface trapping, and the slow part τ_2 represents the radiative recombination [51]. The fitted itemized results of the $(\text{PEA})_2\text{PbI}_4$ films are summarized in Table 2. From the fitted data, the mean recombination lifetimes (τ_{ave}) is calculated by the following equation [52, 53]:

$$\tau_{\text{ave}} = (A_1 \tau_1^2 + A_2 \tau_2^2) / (A_1 \tau_1 + A_2 \tau_2)$$

It can be obtained that the PL lifetime of the pristine film has a fast decay component $\tau_1 = 0.573$ ns, and a slow decay component $\tau_2 = 3.34$ ns ($\tau_{\text{ave}} = 1.71$ ns). Correspondingly, the

Table 2 Fitted PL decay lifetimes of $(\text{PEA})_2\text{PbI}_4$ films fabricated with different concentrations of PVP and PEO polymers

	A_1	τ_1 (ns)	A_2	τ_2 (ns)	τ_{avg} (ns)
$(\text{PEA})_2\text{PbI}_4$	1897.5	0.573	233.11	3.340	1.78
$(\text{PEA})_2\text{PbI}_4/05\%\text{PVP}$	1914.8	0.588	571.6	3.564	2.53
$(\text{PEA})_2\text{PbI}_4/15\%\text{PVP}$	2210.8	0.601	1448.8	3.640	3.07
$(\text{PEA})_2\text{PbI}_4/25\%\text{PVP}$	1795.7	0.583	764.8	3.825	2.96
$(\text{PEA})_2\text{PbI}_4/05\%\text{PEO}$	2151.3	0.588	793.9	3.509	2.59
$(\text{PEA})_2\text{PbI}_4/15\%\text{PEO}$	2272.8	0.583	636.1	3.660	2.56
$(\text{PEA})_2\text{PbI}_4/25\%\text{PEO}$	1840.2	0.608	930.1	3.828	3.08

fast and slow decay components increase after incorporating the various proportions of PVP and PEO polymers, reaching the values of $\tau_1 = 0.583$ ns, $\tau_2 = 3.825$ ns ($\tau_{\text{avg}} = 3.63$ ns) for

PVP-mixed $(\text{PEA})_2\text{PbI}_4$ films, and $\tau_1 = 0.583$ ns, $\tau_2 = 3.66$ ns ($\tau_{\text{avg}} = 3.16$ ns) for PEO-mixed $(\text{PEA})_2\text{PbI}_4$ films, respectively. The average PL lifetimes of the $(\text{PEA})_2\text{PbI}_4$ films increase after introducing the PVP and PEO. These results indicate that the non-radiative recombination is reduced in the polymer-mixed perovskite films, which demonstrate the mechanism proposed above [54, 55].

4 Conclusion

In conclusion, PVP and PEO mixed $(\text{PEA})_2\text{PbI}_4$ films have been fabricated by the spin-coating method. The polymer-mixed $(\text{PEA})_2\text{PbI}_4$ films exhibit improved morphology with more uniform and homogeneous surfaces, which increases with the concentrations of the polymers. XRD and FTIR analyses confirm that the crystal structure and functional group of the pure film don't vary after mixing PVP and PEO polymers. The optical bandgap of the $(\text{PEA})_2\text{PbI}_4$ film was 2.334 eV, which increased to 2.348 eV and 2.343 eV of the $(\text{PEA})_2\text{PbI}_4/25\%$ PVP and $(\text{PEA})_2\text{PbI}_4/25\%$ PEO, respectively. Moreover, the TPL emission of the $(\text{PEA})_2\text{PbI}_4$ films is demonstrated to originate from the exciton recombination, which has been boosted by 3.5 and 3.8 folds by mixing with 25% PVP and 25% PEO, respectively. Time-resolved PL measurements indicate that the PL lifetimes of the polymer-mixed $(\text{PEA})_2\text{PbI}_4$ films have been increased, demonstrating that the increased TPL emission is due to the improved crystalline quality and decreased trap states. This work provides an effective strategy to improve the crystalline quality and photoemission of the 2D perovskite films, which shows great promise for manufacturing high-performance optoelectronic devices based on 2D perovskites.

Acknowledgements This work was supported by the National Natural Science Foundation of China (Nos. 11804109, 11204097 and 11674117). We acknowledge the Analytical & Testing Center of Huazhong University of Science and Technology (HUST) for XRD measurements.

References:

1. W.S. Yang, J.H. Noh, N.J. Jeon, Y.C. Kim, S. Ryu, J. Seo et al., High-performance photovoltaic perovskite layers fabricated through intramolecular exchange. *Science* **348**, 1234–1237 (2015)
2. J. Song, J. Li, X. Li, L. Xu, Y. Dong, H. Zeng, Quantum dot light-emitting diodes based on inorganic perovskite cesium lead halides (CsPbX_3). *Adv. Mater.* **27**, 7162–7167 (2015)
3. M.A. Green, A. Ho-Baillie, H.J. Snaith, The emergence of perovskite solar cells. *Nat. Photonics* **8**, 506–514 (2014)
4. H. Zhou, Q. Chen, G. Li, S. Luo, T.-B. Song, H.-S. Duan et al., Interface engineering of highly efficient perovskite solar cells. *Science* **345**, 542–546 (2014)
5. X. Li, W. Liu, Y. Song, H. Long, K. Wang, B. Wang et al., Two-photon-pumped high-quality, single-mode vertical cavity lasing based on perovskite monocrystalline films. *Nano Energy* **68**, 104334 (2020)
6. J. Yang, B.D. Siempelkamp, D. Liu, T.L. Kelly, Investigation of $\text{CH}_3\text{NH}_3\text{PbI}_3$ degradation rates and mechanisms in controlled humidity environments using in situ techniques. *ACS Nano* **9**, 1955–1963 (2015)
7. F. Yang, M.A. Kamarudin, G. Kapil, D. Hirotani, P. Zhang, C.H. Ng et al., Magnesium-doped MAPbI_3 perovskite layers for enhanced photovoltaic performance in humid air atmosphere. *ACS Appl. Mater. Interfaces* **10**, 24543–24548 (2018)
8. K. Zheng and T. n. Pullerits, "Two dimensions are better for perovskites," ed: ACS Publications, 2019.
9. Y. Zhang, R. Wang, Y. Li, Z. Wang, S. Hu, X. Yan et al., Optical properties of two-dimensional perovskite films of $(\text{C}_6\text{H}_5\text{C}_2\text{H}_4\text{NH}_3)_2[\text{PbI}_4]$ and $(\text{C}_6\text{H}_5\text{C}_2\text{H}_4\text{NH}_3)_2(\text{CH}_3\text{NH}_3)_2[\text{Pb}_3\text{I}_{10}]$. *J. Phys. Chem. Lett.* **10**, 13–19 (2018)
10. Y.-H. Chang, J.-C. Lin, Y.-C. Chen, T.-R. Kuo, D.-Y. Wang, Facile synthesis of two-dimensional Ruddlesden-popper perovskite quantum dots with fine-tunable optical properties. *Nanoscale Res. Lett.* **13**, 1–7 (2018)
11. L. Dou, A.B. Wong, Y. Yu, M. Lai, N. Kornienko, S.W. Eaton et al., Atomically thin two-dimensional organic-inorganic hybrid perovskites. *Science* **349**, 1518–1521 (2015)
12. G. Lanty, A. Brehier, R. Parashkov, J.-S. Lauret, E. Deleporte, Strong exciton–photon coupling at room temperature in microcavities containing two-dimensional layered perovskite compounds. *New J. Phys.* **10**, 065007 (2008)
13. D. Giovanni, W.K. Chong, H.A. Dewi, K. Thirumal, I. Neogi, R. Ramesh et al., Tunable room-temperature spin-selective optical Stark effect in solution-processed layered halide perovskites. *Sci. Adv.* **2**, e1600477 (2016)
14. F. Saouma, C. Stoumpos, J. Wong, M. Kanatzidis, J. Jang, Selective enhancement of optical nonlinearity in two-dimensional organic-inorganic lead iodide perovskites. *Nat. Commun.* **8**, 1–8 (2017)
15. Y.-Q. Zhao, Q.-R. Ma, B. Liu, Z.-L. Yu, J. Yang, M.-Q. Cai, Layer-dependent transport and optoelectronic property in two-dimensional perovskite: $(\text{PEA})_2\text{PbI}_4$. *Nanoscale* **10**, 8677–8688 (2018)
16. D. Liang, Y. Peng, Y. Fu, M.J. Shearer, J. Zhang, J. Zhai et al., Color-pure violet-light-emitting diodes based on layered lead halide perovskite nanoplates. *ACS Nano* **10**, 6897–6904 (2016)
17. H. Zheng, G. Liu, L. Zhu, J. Ye, X. Zhang, A. Alsaedi et al., The Effect of hydrophobicity of ammonium salts on stability of quasi-2d perovskite materials in moist condition. *Adv. Energy Mater.* **8**, 1800051 (2018)
18. L. Qian, Y. Sun, M. Sun, Z. Fang, L. Li, D. Xie et al., 2D perovskite microsheets for high-performance photodetectors. *J. Mater. Chem. C* **7**, 5353–5358 (2019)
19. W.-J. Wei, X.-X. Jiang, L.-Y. Dong, W.-W. Liu, X.-B. Han, Y. Qin et al., Regulating second-harmonic generation by van der Waals interactions in two-dimensional lead halide perovskite nanosheets. *J. Am. Chem. Soc.* **141**, 9134–9139 (2019)
20. S.D. Stranks, V.M. Burlakov, T. Leijtens, J.M. Ball, A. Goriely, H.J. Snaith, Recombination kinetics in organic-inorganic perovskites: excitons, free charge, and subgap states. *Phys. Review Appl.* **2**, 034007 (2014)
21. K. Gauthron, J. Lauret, L. Doyennette, G. Lanty, A. Al Choueiry, S. Zhang et al., Optical spectroscopy of two-dimensional layered $(\text{C}_6\text{H}_5\text{C}_2\text{H}_4\text{-NH}_3)_2\text{-PbI}_4$ perovskite. *Opt. Express* **18**, 5912–5919 (2010)
22. Y. Song, W. Liu, C. Fang, D. Li, P. Lu, Enhanced optoelectronic performance of 2D organic-inorganic hybrid perovskite through light-illumination. *Opt. Express* **27**, 30618–30628 (2019)
23. X. Yang, X. Zhang, J. Deng, Z. Chu, Q. Jiang, J. Meng et al., Efficient green light-emitting diodes based on quasi-two-dimensional

- composition and phase engineered perovskite with surface passivation. *Nat. Commun.* **9**, 1–8 (2018)
24. J. Yao, H. Wang, P. Wang, R.S. Gurney, A. Intaniwet, P. Ruankham et al., Trap passivation and efficiency improvement of perovskite solar cells by a guanidinium additive. *Mater. Chem. Front.* **3**, 1357–1364 (2019)
 25. K. Kim, J. Han, S. Maruyama, M. Balaban, I. Jeon, Role and contribution of polymeric additives in perovskite solar cells: crystal growth templates and grain boundary passivators. *Solar RRL* **5**, 2000783 (2021)
 26. C.-Y. Chang, C.-Y. Chu, Y.-C. Huang, C.-W. Huang, S.-Y. Chang, C.-A. Chen et al., Tuning perovskite morphology by polymer additive for high efficiency solar cell. *ACS Appl. Mater. Interfaces* **7**, 4955–4961 (2015)
 27. M. Yavari, M. Mazloum-Ardakani, S. Gholipour, M.M. Tavakoli, N. Taghavinia, A. Hagfeldt et al., Reducing surface recombination by a poly (4-vinylpyridine) interlayer in perovskite solar cells with high open-circuit voltage and efficiency. *ACS Omega* **3**, 5038–5043 (2018)
 28. C.-H. Gao, Y. Zhang, X.-J. Ma, F.-X. Yu, Y.-L. Jia, Y.-L. Lei et al., A method towards 100% internal quantum efficiency for all-inorganic cesium halide perovskite light-emitting diodes. *Org. Electron.* **58**, 88–93 (2018)
 29. Y. Mei, M. Sun, H. Liu, X. Li, and S. Wang (2021), "Polymer additive assisted crystallization of perovskite films for high-performance solar cells," *Org. Electron.* 106258.
 30. D. Wang, L. Zhang, K. Deng, W. Zhang, J. Song, J. Wu et al., Influence of polymer additives on the efficiency and stability of ambient-air solution-processed planar perovskite solar cells. *Energ. Technol.* **6**, 2380–2386 (2018)
 31. H. Zheng, L. Zhu, L. Hu, S. Yang, S. Chen, A. Alsaedi et al., Promoting perovskite crystal growth to achieve highly efficient and stable solar cells by introducing acetamide as an additive. *J. Mater. Chem. A* **6**, 9930–9937 (2018)
 32. Y. Liu, H. Ye, Y. Zhang, K. Zhao, Z. Yang, Y. Yuan et al., Surface-tension-controlled crystallization for high-quality 2D perovskite single crystals for ultrahigh photodetection. *Matter* **1**, 465–480 (2019)
 33. Y. Song, C. Zhang, W. Liu, X. Li, H. Long, K. Wang et al., High-efficiency energy transfer in perovskite heterostructures. *Opt. Express* **26**, 18448–18456 (2018)
 34. M.-G. La-Placa, D. Guo, L. Gil-Escrig, F. Palazon, M. Sessolo, H.J. Bolink, Dual-source vacuum deposition of pure and mixed halide 2D perovskites: thin film characterization and processing guidelines. *J. Mater. Chem. C* **8**, 1902–1908 (2020)
 35. B.A. Al-Asbahi, S.M. Qaid, M. Hezam, I. Bedja, H.M. Ghaithan, A.S. Aldwayyan, Effect of deposition method on the structural and optical properties of CH₃NH₃PbI₃ perovskite thin films. *Op. Mater.* **103**, 109836 (2020)
 36. A. El-naggar, M. Osman, Z.K. Heiba, M.B. Mohamed, A. Kamal, A. Aldhafiri et al., Effect of chlorobenzene on the optical and structural properties of CH₃NH₃PbI₃: DMF perovskite films. *J. Mater. Res.* **14**, 287–297 (2021)
 37. F. Li, Y. Pei, F. Xiao, T. Zeng, Z. Yang, J. Xu et al., Tailored dimensionality to regulate the phase stability of inorganic cesium lead iodide perovskites. *Nanoscale* **10**, 6318–6322 (2018)
 38. J. Chen, D. Lee, N.-G. Park, Stabilizing the Ag electrode and reducing J-V hysteresis through suppression of iodide migration in perovskite solar cells. *ACS Appl. Mater. Interfaces* **9**, 36338–36349 (2017)
 39. J. Gong, M. Yang, D. Rebollar, J. Rucinski, Z. Liveris, K. Zhu et al., Divalent anionic doping in perovskite solar cells for enhanced chemical stability. *Adv. Mater.* **30**, 1800973 (2018)
 40. W.J. Mir, T. Sheikh, H. Arfin, Z. Xia, A. Nag, Lanthanide doping in metal halide perovskite nanocrystals: spectral shifting, quantum cutting and optoelectronic applications. *NPG Asia Mater.* **12**, 1–9 (2020)
 41. Y. Liu, Y. Zhang, Z. Yang, H. Ye, J. Feng, Z. Xu et al., Multi-inch single-crystalline perovskite membrane for high-detectivity flexible photosensors. *Nat. Commun.* **9**, 1–11 (2018)
 42. H. Xiong, G. DeLuca, Y. Rui, B. Zhang, Y. Li, Q. Zhang et al., Modifying perovskite films with polyvinylpyrrolidone for ambient-air-stable highly bendable solar cells. *ACS Appl. Mater. Interfaces* **10**, 35385–35394 (2018)
 43. X. Hong, T. Ishihara, A. Nurmikko, Dielectric confinement effect on excitons in PBI 4-based layered semiconductors. *Phys. Rev. B* **45**, 6961 (1992)
 44. J. Zhang, X. Zhu, M. Wang, B. Hu, Establishing charge-transfer excitons in 2D perovskite heterostructures. *Nat. Commun.* **11**, 1–8 (2020)
 45. Y. Song, W. Liu, Y. Qin, X. Han, W. Li, X. Li et al., Photoinduced trap passivation for enhanced photoluminescence in 2D organic–inorganic hybrid perovskites. *Adv. Opt. Mater.* **8**, 1901695 (2020)
 46. J. Di, M. Zhong, Y. Wang, Polyvinylpyrrolidone/polyvinyl alcohol blends modification on light absorbing layer to improve the efficiency and stability of perovskite solar cells. *Mater. Sci. Semicond. Process.* **133**, 105941 (2021)
 47. C. Wu, Y. Zou, T. Wu, M. Ban, V. Pecunia, Y. Han et al., Improved performance and stability of all-inorganic perovskite light-emitting diodes by antisolvent vapor treatment. *Adv. Func. Mater.* **27**, 1700338 (2017)
 48. W.K. Chong, K. Thirumal, D. Giovanni, T.W. Goh, X. Liu, N. Mathews et al., Dominant factors limiting the optical gain in layered two-dimensional halide perovskite thin films. *Phys. Chem. Chem. Phys.* **18**, 14701–14708 (2016)
 49. W. Liu, X. Li, Y. Song, C. Zhang, X. Han, H. Long et al., Cooperative enhancement of two-photon-absorption-induced photoluminescence from a 2D perovskite-microsphere hybrid dielectric structure. *Adv. Func. Mater.* **28**, 1707550 (2018)
 50. X. Wu, M.T. Trinh, D. Niesner, H. Zhu, Z. Norman, J.S. Owen et al., Trap states in lead iodide perovskites. *J. Am. Chem. Soc.* **137**, 2089–2096 (2015)
 51. Y. Ling, L. Tan, X. Wang, Y. Zhou, Y. Xin, B. Ma et al., Composite perovskites of cesium lead bromide for optimized photoluminescence. *J. Phys. Chem. Lett.* **8**, 3266–3271 (2017)
 52. P. Chen, Y. Bai, S. Wang, M. Lyu, J.H. Yun, L. Wang, In situ growth of 2D perovskite capping layer for stable and efficient perovskite solar cells. *Adv. Func. Mater.* **28**, 1706923 (2018)
 53. J. Yan, B. Zhang, Y. Chen, A. Zhang, X. Ke, Improving the photoluminescence properties of perovskite CH₃NH₃PbBr 3-xCl x films by modulating organic cation and chlorine concentrations. *ACS Appl. Mater. Interfaces* **8**, 12756–12763 (2016)
 54. J. Peng, Y. Wu, W. Ye, D.A. Jacobs, H. Shen, X. Fu et al., Interface passivation using ultrathin polymer–fullerene films for high-efficiency perovskite solar cells with negligible hysteresis. *Energy Environ. Sci.* **10**, 1792–1800 (2017)
 55. Q. Jiang, Y. Zhao, X. Zhang, X. Yang, Y. Chen, Z. Chu et al., Surface passivation of perovskite film for efficient solar cells. *Nat. Photonics* **13**, 460–466 (2019)

Publisher's Note Springer Nature remains neutral with regard to jurisdictional claims in published maps and institutional affiliations.